# Eruption of a boundary layer induced by a 2D vortex patch



2009 Fluid Dyn. Res. 41 055502

(http://iopscience.iop.org/1873-7005/41/5/055502)

IOP PUBLISHING FLUID DYNAMICS RESEARCH

Fluid Dyn. Res. **41** (2009) 055502 (18pp) doi:10.1088/0169-5983/41/5/055502

# Eruption of a boundary layer induced by a 2D vortex patch

**H Kudela**[1] **and Z M Malecha**

Faculty of Mechanical and Power Engineering, Wroclaw University of Technology, ul. Wybrzeze Wyspianskiego 27, Wroclaw, Poland

E-mail: henryk.kudela@pwr.wroc.pl

Received 16 February 2009, in final form 18 August 2009
Published 14 September 2009
Online at stacks.iop.org/FDR/41/055502

Communicated by G Vallis

**Abstract**

The boundary-layer eruption phenomenon caused by a 2D patch of vorticity above a wall was investigated. It is shown that the eruption phenomenon depends on the viscosity (or Reynolds number, *Re*) of the fluid. There exists a threshold value of *Re* above which the eruption takes place. The initiation of the eruption goes through the creation of a small recirculation zone near the solid wall, the appearance of the saddle point on streamlines inside it and the tearing off process of the recirculation zone. Further increase of the Reynolds number causes a more complex flow. One can observe that eruption is regenerative and that the vortex patch can produce a cascade of secondary vortices. The vortex-in-cell method was employed to investigate the eruption phenomenon.

## 1. Introduction

The processes involved in unsteady boundary-layer separation are important in understanding the self-sustaining mechanism of near-wall turbulence (Panton 2001, Perry and Chong 1982). Especially important are the processes related to the regeneration of turbulence in the boundary layer. The regeneration mechanism is connected with the breakdown in the boundary layer and the intense eruption of vorticity from the wall. In an incompressible flow, vorticity can be generated only on the rigid wall.

Vortex production on the wall is forced by the fluid viscosity (no-slip condition) in conjunction with the effect of the pressure gradient on the boundary. The production of vorticity on the wall can be interpreted as necessary for the no-slip condition (Batchelor 1970, Bradshaw 1996). Introduction of vorticity from the wall can take place through short-range

[1] Author to whom any correspondence should be addressed.


0169-5983/09/055502+18$30.00

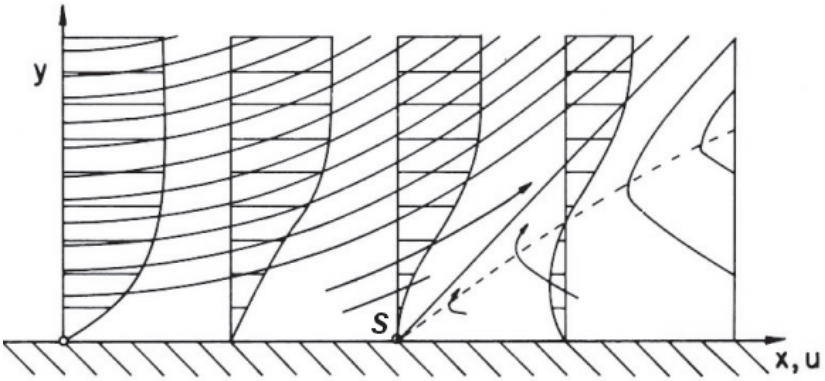


**Figure 1.** Prandtl's sketch of the streamlines and velocity profiles in the vicinity of the separation point. At the stagnation point **S**, the shear stress $\tau_s = \frac{\partial u}{\partial y} = 0$. On the right of the stagnation point, reverse flow is established.

diffusion, as in laminar flow, or can happen abruptly through vorticity eruption from the wall layer (Kudela and Malecha 2007, Smith and Walker 1996). Here, 'eruption' means sudden injection of vorticity generated near the wall into the outer region. This process feeds the outer region with a new portion of concentrated vorticity.

In this paper, to gain some idea about the regeneration mechanism of the vorticity production on the wall, we investigated numerically the two-dimensional (2D) viscous vortex patch interaction with the wall. We used the vortex particle method that is well suited for problems where evolution of vorticity is important. The eruption phenomenon is linked to the process known as separation of the boundary layer, which has already been described by Prandtl (1905). Separation is a notion used to describe both steady and unsteady flows, and that is why its meaning is not clear. In a steady flow the body surface is also a streamline. The velocity of the fluid on the wall equals zero, but it has a nonzero value at an arbitrarily small distance from the wall.

The process of separation takes place when two fluid particles with opposite velocity vectors meet at one point on the wall (figure 1). As described by Prandtl, such a situation occurs when a positive pressure gradient appears near the wall driving the flow in the direction opposite to the mainstream.

The point where meeting fluid particles begin to depart from the plane wall is called the separation point. If we denote velocity components along the wall by $u$, and those perpendicular to it by $v$, then at the separation point the shear stress equals zero:

$$\frac{\partial u}{\partial y} = 0, \quad \text{at } y = 0. \tag{1}$$

The condition above is important for steady flows with low Reynolds number. It was demonstrated for the first time by Prandtl (Prandtl 1905, Schlichting 1979). When analysing the motion using Prandtl's steady boundary-layer equations, it can be demonstrated that condition (1) leads to the appearance of a singularity, which means that the normal velocity component $v$ at the separation point approaches infinity (Landau and Lifszyc 1994). The appearance of the singularity indicates that the fluid in the boundary layer will penetrate the flow domain much farther than is found from the boundary-layer thickness estimation. Prandtl described this phenomenon in the following way (Telionis 1981): 'a fluid sheet projects itself into the free flow and affects a complete alteration of the motion'.

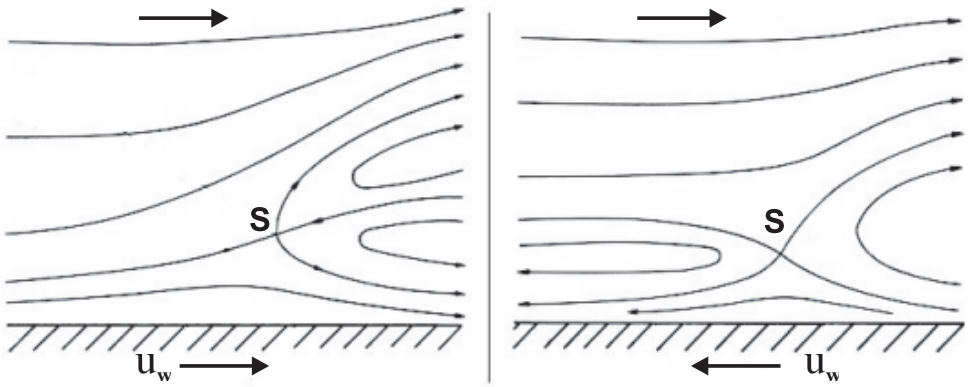


**Figure 2.** The streamline pattern at the point of separation **S** caused by a downstream moving wall (left) and an upstream moving wall (right) with velocity $u_w$. The separation point is established within the flow (MRS condition).

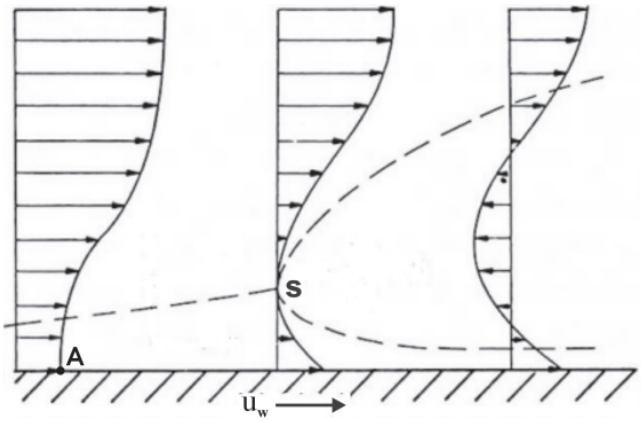


**Figure 3.** Velocity profiles over the moving wall corresponding to the streamlines from the left panel of figure 2. At the point **A**, $\tau_s = 0$, but there is no separation point. The separation point **S** appears within the flow and fulfils condition (2). The dashed line represents the streamlines (Telionis 1981).

Moore, Rott and Sears (MRS) (Rott 1956, Sears 1956, Telionis 1981) quoted arguments indicating that condition (1) is insufficient for unsteady flows. According to MRS, the actual transfer of fluid particles from the wall region takes place when the stagnation point and the point of zero stress are located within the flow as shown in figures 2 and 3:

$$\frac{\partial u}{\partial y} = 0, \quad \text{and} \quad u = 0. \tag{2}$$

Figure 2 shows the schematics of streamlines in the vicinity of the separation point **S** when the wall moves with velocity $u_w$ with the mainstream or against it. In such a case, it is said that the separation point satisfies the MRS condition. For the streamlines, it is a saddle point. Figure 3 shows velocity profiles corresponding to the streamlines in figure 2 (Telionis 1981).

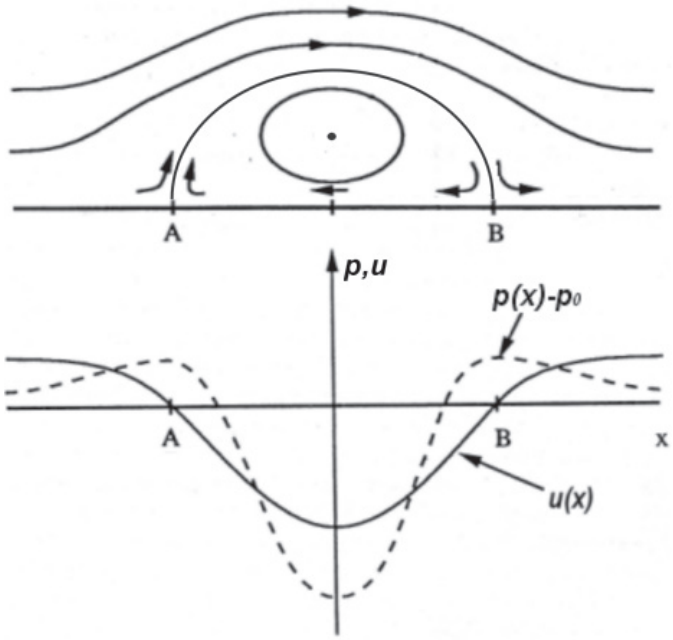


**Figure 4.** Streamline pattern caused by the point vortex. One can note the recirculation zone with the two stagnation points **A** and **B**. The graph beneath shows distribution of the pressure $p(x) - p_0$ (where $p_0$ is the pressure at infinity) and the velocity $u(x)$ along the wall (Smith and Walker 1996).

The canonical problem leading to the abrupt eruption of the boundary layer is the interaction of a point vortex with the viscous boundary layer (Doligalski and Walker 1984, Doligalski *et al* 1994, Smith and Walker 1996, Walker 1978). In these works, the point vortex was moving in a uniform flow in the vicinity of the plain wall. The vortex was inducing, on its right side, motion toward the wall and, on its left side, motion away from the wall. This caused a recirculation zone with the two stagnation points **A** and **B** (adverse flow) close to the wall to appear (figure 4). It could be observed that the maximum negative value of the velocity and the absolute minimum in pressure were both directly under the centre of the vortex. On the left of this point, the mainstream velocity was increasing monotonically to zero at the stagnation point. The pressure was increasing with velocity; so to the left of the vortex, an adverse pressure gradient was established.

In the present paper, the point vortex was replaced by a small area of concentrated vorticity (a thick vortex core). The research presented here will be dealing with the interactions of a 2D vortex patch with the wall for different values of fluid viscosity (Reynolds number). The 2D equation of the viscous fluid motion will be solved. The interaction of the 2D vortex patch and the wall can be considered as a simplified model of the interaction between the 3D vortex and the wall. In such a case, the vortex patch can be understood as a cross section of the 3D streamwise vortex (figure 5) (Jimenez and Moin 1991, Panton 2001, Robinson 1991).

In a previous paper (Kudela and Malecha 2007), we showed the eruption of the boundary-layer phenomenon provoked by the vortex patch but only for one value of the viscosity. The viscosity was simulated by the random walk method. In the present paper, we have applied the particle strength exchange (PSE) method to model viscosity and significantly improved the computational procedure.

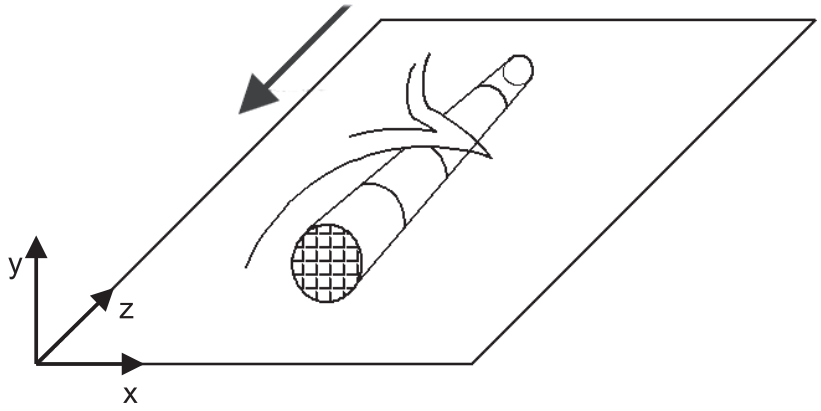


**Figure 5.** Schematics of a streamwise vortex. The cross section of the streamwise vortex with the $(x, y)$ plane can be considered as a vortex patch.

## 2. The equations of motion

The equations of 2D motion of the viscous, incompressible and constant density fluid are as follows:

$$\frac{\partial \boldsymbol{u}}{\partial t} + (\boldsymbol{u} \cdot \nabla)\, \boldsymbol{u} = -\frac{1}{\rho} \nabla p + \nu \Delta \boldsymbol{u}, \tag{3}$$

$$\frac{\partial u}{\partial x} + \frac{\partial v}{\partial y} = 0, \tag{4}$$

where $\boldsymbol{u} = (u, v)$ is the velocity vector, $\rho$ is the density of the fluid, $\nu$ is the kinematic viscosity coefficient, $p$ is the pressure and $\Delta = \frac{\partial^2}{\partial x^2} + \frac{\partial^2}{\partial y^2}$ is the Laplace operator.

Equations (3) and (4) must be complemented by the initial and boundary conditions, which in this case are

$$\boldsymbol{u} = 0, \quad \text{for } (x, y) \in \partial\Omega, \tag{5}$$

$$\boldsymbol{u}(\boldsymbol{x}, 0) = \boldsymbol{u}_0(x, y), \tag{6}$$

where $\partial\Omega$ means the rigid wall and $\boldsymbol{u}_0(x, y)$ is the initial velocity distribution. In this case, the initial velocity is the velocity field of the isolated vortex patch. Equation (4) expresses the incompressibility of the flow and guarantees the existence of the stream function $\psi$, which is related to the velocity field in the following way: $u = \psi_y$ and $v = -\psi_x$.

In 2D space, the vorticity vector $\mathrm{rot}(\boldsymbol{u}) = \boldsymbol{k}\omega = \partial_x v - \partial_y u$ has only one nonzero component perpendicular to the plane of motion ($\boldsymbol{k}$ is a unit vector, perpendicular to the plane of motion). Acting with the rotation operator $\mathrm{rot}(\cdot)$ on both sides of expression (3), this equation can be transformed into the Helmholtz equation describing the evolution of the vorticity field in time:

$$\omega_t + u\omega_x + v\omega_y = \nu \Delta \omega, \tag{7}$$

$$\Delta \psi = -\omega; \quad u = \psi_y, \quad v = -\psi_x. \tag{8}$$

Vector equation (3) has been replaced with scalar equation (7) for $\omega(x, y, t)$. It is worth noting that in equation (7) there is no pressure term.

In vortex methods, the viscosity decomposition algorithm is commonly used (Cottet and Koumoutsakos 2000). This means that equation (7) is solved in two steps: first the inviscid equation:

$$\omega_t + u\omega_x + v\omega_y = 0 \tag{9}$$

and then the viscous diffusion equation (the Stokes problem):

$$\omega_t = \nu\Delta\omega. \tag{10}$$

In this paper, equations (9) and (10) were solved by the vortex particle method.

## 3. Description of the vortex particle method

From equation (9), it can be deduced that the vorticity is constant along the trajectories of the fluid material particles ($\mathrm{d}\omega/\mathrm{d}t = 0$). So $\omega(\boldsymbol{x}(t, \boldsymbol{\alpha}), t) = \omega(\boldsymbol{\alpha}, 0)$, where $\boldsymbol{x}(t, \alpha)$ denotes the position at time $t$ of the particle, which at the initial instant $t = 0$ was in the position $\boldsymbol{\alpha}$. According to the third Helmholtz theorem (Wu *et al* 2006), vorticity lines move with the (ideal) fluid. This means that the movement of vortex particles can be described by the infinite set of ordinary differential equations:

$$\frac{\mathrm{d}\boldsymbol{x}_p}{\mathrm{d}t} = \boldsymbol{u}(\boldsymbol{x}_\mathrm{p}, t), \quad \boldsymbol{x}(0, \boldsymbol{\alpha}) = \boldsymbol{\alpha}, \tag{11}$$

where $\boldsymbol{\alpha} = (\alpha_1, \alpha_2)$ means the Lagrange coordinates of fluid particles.

By solving the Poisson equation for the stream function (8) and differentiating, the velocity field can be presented as dependent on the vorticity distribution:

$$\boldsymbol{u}(\boldsymbol{x}) = \int \mathrm{K}(\boldsymbol{x} - \boldsymbol{x}')\omega(\boldsymbol{x},' t)\,\mathrm{d}\boldsymbol{x}', \tag{12}$$

where

$$\mathrm{K}(\boldsymbol{x}) = \frac{1}{2\pi|\boldsymbol{x}|}(-y, x), \quad \text{and} \quad |\boldsymbol{x}| = \sqrt{x^2 + y^2}.$$

Equation (12) is a fundamental formula for direct vorticity methods (Chorin 1973). The velocity field can also be determined by solving the Poisson equation for the stream function (8) on the numerical mesh by a finite difference method. Subsequently, the velocity from the mesh nodes is interpolated onto the particle's positions. Such an approach significantly accelerates the calculations, and for this reason it was used in this work (Cottet and Koumoutsakos 2000).

For the sake of numerical calculations, it was necessary to replace the infinite set of differential ordinary equations (11) with the finite set. In order to achieve it, the space of Lagrange variables is covered by a regular mesh $(j_1\Delta x, j_2\Delta y)$, $(j_1, j_2 = 1, \ldots, N)$, $\Delta x = \Delta y = h$. The mesh is also used to solve the Poisson equation for the stream function. In the present method, the initial vorticity field is replaced by a distribution of vortex particles. To each particle circulation is assigned

$$\Gamma_p(\boldsymbol{x}_p) = \int_{A_p} \omega\,(x, y)\,\mathrm{d}A \approx h^2\bar{\omega}, \tag{13}$$

where $A_p = h^2$ denotes the cell area with index $p = (j_1, j_2)$, whereas $\bar{\omega}$ is the mean vorticity value for the cell. Vorticity is approximated by the sum of Dirac discrete measures

$$\omega(\boldsymbol{x}) \approx \sum_{i=1}^{N} \Gamma \delta(\boldsymbol{x} - \boldsymbol{x}_p), \tag{14}$$

where $N$ is the number of particles and $\delta$ denotes the Dirac function. Circulations of particles change with time as a result of diffusion. The solution of equation (9) in the time interval $(t_n, t_{n+1})$ is obtained by solving a set of differential equations:

$$\frac{\mathrm{d}\boldsymbol{x}_p}{\mathrm{d}t} = \boldsymbol{u}(\boldsymbol{x}_p^n(t), t), \quad \boldsymbol{x}_p(t_n) = \boldsymbol{x}_p^n, \quad t_n \leqslant t \leqslant t_{n+1}, \quad p = 1, \ldots, N \tag{15}$$

and new positions of the particles are approximate solutions of equation (9) for the time $t = t^{n+1}$:

$$\omega^{n+1}(\boldsymbol{x}) = \sum_{p=1}^{N} \Gamma_p \delta(\boldsymbol{x} - \boldsymbol{x}_p^{n+1}), \quad \boldsymbol{x}_p^{n+1} = \boldsymbol{x}_p(t_{n+1}). \tag{16}$$

To solve the diffusion equation (10), the PSE method was used. The main idea of the PSE method is to replace the differential Laplace operator by the integral operator $\Delta_\epsilon$ (Cottet and Koumoutsakos 2000):

$$\Delta_\epsilon(\boldsymbol{x}) \cong \frac{1}{\epsilon^2} \int (\omega(\boldsymbol{y}) - \omega(\boldsymbol{x}))\eta_\epsilon(\boldsymbol{y} - \boldsymbol{x})\,\mathrm{d}\boldsymbol{y}. \tag{17}$$

The function $\eta_\epsilon = \epsilon^{-2}(x/\epsilon)$, $(\epsilon > 0)$, is a symmetric cut-off function satisfying specific conditions for its moments. For the PSE method to be effective, the relation $\epsilon/h \geqslant 1$, where $h$ is the cell size, must be satisfied, i.e. the supports of adjacent particles must overlap. In practice, this means that each particle should be able to communicate with a certain number of adjacent particles. Using (17) the change of the particle intensity due to viscosity can be expressed as:

$$\frac{\mathrm{d}\Gamma_p}{\mathrm{d}t} = \nu\epsilon^{-2} \sum_q (\Gamma_q - \Gamma_p)\,\eta\left(\frac{\boldsymbol{x}_p - \boldsymbol{x}_q}{\epsilon}\right). \tag{18}$$

The function $\eta(\boldsymbol{x})$ can have infinite support; however, such a function has a major disadvantage: it requires calculating the interaction of each vortex particle with all other particles in the flow domain. It means that computational effort is proportional to $O(N^2)$, where $N$ denotes the number of vortex particles in the flow. Quadratic complexity significantly slows down the calculation process. A solution of this problem is to apply the function $\eta(\boldsymbol{x})$ with finite support. In this paper, a second-order function with finite support was chosen:

$$\eta(x) = \begin{cases} \dfrac{C}{1 + |x|^2} & \text{for } |x| \leqslant 2, \\ 0, & \text{for } |x| > 2, \end{cases} \tag{19}$$

where $C = 0.835$ was calculated to satisfy the condition for the second moment, which should be equal to $2(\int x^2\eta(x)\,\mathrm{d}x = 2)$ (Cottet and Koumoutsakos 2000). In the case of a function with finite support, computational effort is proportional to $O(mN)$, where $m$ means the number of particles within the support of the cut-off function. Because $m \ll N$ and $m$ is constant, the computational effort is linear (proportional to $O(N)$). In the algorithm developed for this work, the kernel (support) of the function (19) covered exactly nine neighbouring vortex particles ($m = 9$).

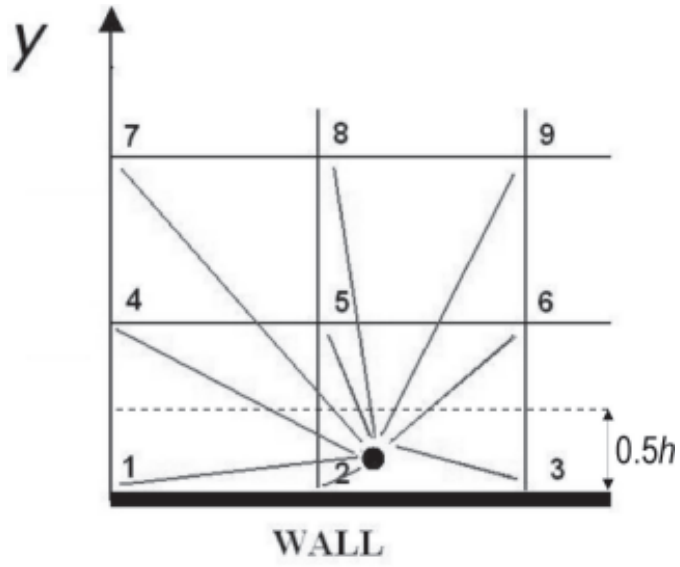


**Figure 6.** Remeshing of vortex particles close to the wall.

Vortex particle methods belong to the class of self-adaptive methods. Vortex particles tend to gather in the regions of high velocity gradients. Particles grouping in some regions is an undesirable phenomenon. It worsens the precision of the viscous effect modelling (solution to the diffusion equation) and it could create phantom vortex structures, which could significantly alter the velocity field. To avoid these problems it is necessary to apply an additional procedure to obtain a uniform distribution of vortex particles in the flow domain. The process is called remeshing. When vortex particles are uniformly distributed, the cut-off function (19) always covers exactly the same number of particles. This can be achieved when remeshing is performed in each time step. In this work, such an approach was adopted. After the advection step vortices were distributed on a regular grid coinciding with the numerical mesh used to solve the Poisson equation (8). Reorganization of the particles' location and circulation was controlled by the second-order interpolation kernel:

$$\varphi(x) = \begin{cases} 1 - x^2, & 0 \leqslant x < \frac{1}{2}, \\ (1-x)(2-x)/2, & \frac{1}{2} \leqslant x < \frac{3}{2}, \\ 0, & x \geqslant \frac{3}{2}. \end{cases} \tag{20}$$

To avoid problems with vorticity 'running out' beyond the boundaries of the calculation domain, the kernel (20) was modified for particles closer to the wall than $\frac{1}{2}h$ (Koumoutsakos 1993) (figure 6):

$$\varphi(x) = \begin{cases} 1 - \frac{3}{2}x + \frac{1}{2}x^2, & \text{for nodes } 1,\ 2,\ 3, \\ x(2-x), & \text{for nodes } 4,\ 5,\ 6, \\ x(x-1), & \text{for nodes } 7,\ 8,\ 9, \\ 0, & \text{for all other nodes.} \end{cases} \tag{21}$$

The 2D interpolation kernel is a product of 1D kernels: $\varphi^*(x, y) = \varphi(x)\varphi(y)$. Finally, the interpolation proceeds as follows:

$$\Gamma_i^*(x_i^*, y_i^*) \approx \sum_{j=1}^{N} \Gamma_j(x_j, y_j)\varphi(x_i^* - x_j)\varphi(y_i^* - y_j), \tag{22}$$

where $\Gamma^*$ denotes new circulation of the vortex particle in its new position $(x_i^*, y_i^*)$.

Because remeshing was performed in each time step, the individual procedure for the redistribution of particles' circulations onto the mesh nodes was unnecessary. It made the whole process of the calculations faster. The differential equation (15) was solved by the second-order Euler-improved method. The velocity of the particles between the grid nodes was calculated using the interpolation formula:

$$\boldsymbol{u}(\boldsymbol{x}_p) = \sum_j \boldsymbol{u}_j l_h(\boldsymbol{x}_p - \boldsymbol{x}_j), \tag{23}$$

where $l_h$ is a basic bilinear Lagrange function.

## 4. Realization of the no-slip condition

Condition (5) for the viscous fluid motion equation implies no slip between the fluid and the wall. Both normal and tangent components of the velocity field should vanish. Describing the fluid motion using vorticity and the stream function simplified the equations of motion, but complicated the realization of the boundary condition (5). In numerical practice of the vortex methods, realization of the condition (5) is achieved by generating the appropriate amount of vorticity on the rigid wall. The wall is treated as a vorticity layer with intensity $\gamma(s, t) = [u_\omega]$, where $u_\omega$ means velocity induced on the wall by the vorticity located inside the flow domain and a square bracket denotes a jump in the velocity value from zero to $u_\omega$. Here, our task is to eliminate the undesirable vorticity layer. The intensity of the vorticity layer can be described by an integral equation that encompasses the entire wall (the global approach). However, this problem can also be treated locally. In this work, Lighthill's approach was adopted (Lighthill 1963). The idea is to satisfy the no-slip condition by assigning a specific value of the vorticity flux $\nu(\partial\omega/\partial n)$. To understand how the vorticity flux can compensate for the undesirable tangent component of the velocity field the equation of the viscous fluid motion on the wall has to be written in the form

$$\frac{\mathrm{d}\boldsymbol{u}}{\mathrm{d}t} \approx \frac{u(t + \Delta t) - u(t)}{\Delta t} = -\frac{\partial p}{\partial s} - \nu\frac{\partial \omega}{\partial n}, \tag{24}$$

where the variable $y$ is in the direction orthogonal to the wall. One can notice that acceleration is related to the pressure gradient as well as to the vorticity flux. If the tangent velocity component appears on the wall, it can be interpreted as additional acceleration generated in a short interval $\Delta t$. This acceleration can be compensated for the additional vorticity flux $\nu(\partial\omega/\partial n)$. Therefore, we can assume that in the time interval $\Delta t$, the tangent velocity component is annihilated by $u_\mathrm{s} = \nu\Delta t\partial_y\omega$. Hence, the derivative of vorticity in the direction perpendicular to the wall is

$$\frac{\partial \omega}{\partial y} = -\frac{\gamma}{\nu\Delta t}, \tag{25}$$

where $\gamma$ is the intensity of the vorticity layer along the wall. To introduce a new vorticity, generated by the vorticity flux, into the flow domain, an additional initial-boundary value

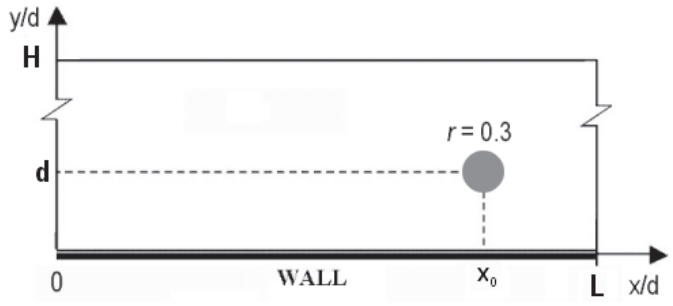


**Figure 7.** Computational domain of the problem.

problem for the diffusion equation must be solved (Koumoutsakon *et al* 1994):

$$\begin{aligned} &\omega_t = \nu\Delta\omega, \\ &\omega(x, y, t = 0) = 0, \\ &\frac{\partial\omega}{\partial y} = -\frac{\gamma}{\nu\Delta t}. \end{aligned} \tag{26}$$

It should be noted that the initial condition for problem (26) is equal to zero. It was solved on the numerical mesh by a finite difference method. Vorticity obtained by solving equation (26) is added to the vorticity already existing in the fluid and converted to particles.

## 5. Numerical calculations

Figure 7 shows the schematics of the computation domain together with a vortex patch, $d$ is the distance between the vortex centre and the wall and $r$ is the vortex radius. The Navier–Stokes equation (3) was transformed into non-dimensional form by introducing as a characteristic length $\bar{L} = d$, velocity $\bar{U} = \Gamma/2\pi r$ and time $\bar{T} = \bar{L}/\bar{U}$. Using non-dimensional variables $\boldsymbol{x}' = \boldsymbol{x}/\bar{L}$, $t' = t/\bar{T}$, $\boldsymbol{u}' = \boldsymbol{u}/\bar{U}$, equation (8) takes the form

$$\omega_t + u\omega_x + v\omega_y = (1/Re)\Delta\omega, \tag{27}$$

where $Re = \frac{\bar{U}\bar{L}}{\nu} = \frac{\Gamma}{2\pi\nu} \cdot \frac{d}{r}$ is the Reynolds number and $\Gamma = \omega_0\pi r^2$, where $\omega_0$ is the initial vorticity of the patch.

The size of the computational domain was chosen by trial and error to minimize the influence of the boundary condition on the numerical results. Finally, for the computational domain was chosen $L = 8$ and $H = 7$ in non-dimensional units. In order to solve the Poisson equation for the stream function, the boundary conditions were as follows: in the direction $x$, a periodic boundary condition was used, whereas for the bottom ($y = 0$) and upper ($y = L$) boundaries, $\psi = 0$ was used. The initial position of the vortex patch was $x_0 = 7.5$, $y_0 = d = 1$, its initial radius was $r = 0.3$ and its vorticity was $\omega_0 = -1.25$. The mesh size and the time step were $\Delta x = \Delta y = 0.01$ and $\Delta t = 0.01$, respectively.

One time step from $t_n$ to $t_n + \Delta t$ proceeded as follows:

1. Redistributing particles' circulations onto the mesh nodes (20) and (21).
2. Solving the Poisson equation for the stream function:

$$\begin{aligned} &\Delta\psi = -\omega, \\ &\psi|_{x=0} = \psi|_{x=L}, \quad \psi|_{y=0} = \psi|_{y=H} = 0. \end{aligned}$$

3. Calculating the velocity on the numerical mesh:

$$u_{i,j} = \frac{\psi(x_i, y_j + \Delta y) - \psi(x_i, y_j - \Delta y)}{2\Delta y},$$

$$v_{i,j} = -\frac{\psi(x_i + \Delta x, y_j) - \psi(x_i - \Delta x, y_j)}{2\Delta x}.$$

4. Determining the vorticity layer $\gamma = u_s$ and the solution of the diffusion equation (26).
5. Displacing vortex particles according to (15).
6. Remeshing vortex particles onto a regular grid (formulae (20) and (21)).
7. Changing the circulations of particles as the result of diffusion by using the PSE method (18).

To solve the stream function equation (8), a fast elliptic equation solver was used. The same program was also adopted to solve the diffusion equation (26). For this purpose, the time derivative was replaced by the difference quotient: $\omega_t|_{t=t^{n+1}} \approx (\omega^{n+1}/\Delta t)$, $(\omega^n = 0)$, which resulted in the elliptic equation:

$$\begin{aligned} &\Delta\omega^{n+1} - \frac{\omega^{n+1}}{\nu\Delta t} = 0, \\ &\frac{\partial\omega}{\partial y}|_{y=0} = -\frac{u_s}{\nu\Delta t}, \quad \omega|_{x=0} = \omega|_{x=L}, \quad \omega|_{y=H} = 0. \end{aligned} \tag{28}$$

## 6. Numerical results

A vortex patch, because of the presence of the wall, moves along it from right to left. The direction of the movement is determined by the sign of vorticity of the patch. The maximum velocity induced by the patch is directly below it, so the pressure in this place has a minimal value. Away from the discussed vortex structure, in the direction of motion, the velocity decreases, while the pressure increases. This means that the pressure gradient is opposite to the horizontal movement of the patch. Such a pressure gradient slows down the fluid motion so that separation points and recirculation zones may appear near the wall. A recirculation zone may precede the occurrence of an unsteady separation event. The emerging boundary recirculation zone resembles a bubble growing bigger in the direction perpendicular to the wall, eventually leading to eruption of the boundary layer.

In figure 8(a), the pattern of streamlines just before the eruption is presented. The figure was obtained by analytic studies of Prandtl's boundary layer equations (Cowley *et al* 1990, Doligalski *et al* 1994, Smith and Walker 1996). Zone I presents the viscous boundary layer. In zone II, the flow direction is opposite to the mainstream direction and is treated as irrotational (Cowley *et al* 1990). This zone separates two zones, I and III, and controls the eruption (Peridier *et al* 1991a, 1991b). In figure 8(b), we present the streamlines and the direction of flow near the region of boundary layer separation obtained in our computations. In the background of the streamlines, the vorticity field is marked. The dark (light) colour represents positive (negative) vorticity. The recirculation zone with two stagnation points, marked **A** and **B**, is clearly visible. It should be noted that the initial vortex patch that induced the recirculation zone is not visible in figure 8(b) because it is located above. Point **A** is an attachment point. At the point **B**, fluid particles with opposite velocity vectors meet and they depart from the wall. This point is a separation point (shear stress on the wall disappears, $\partial u/\partial y = 0$), but here eruption of the boundary layer does not take place. According to the

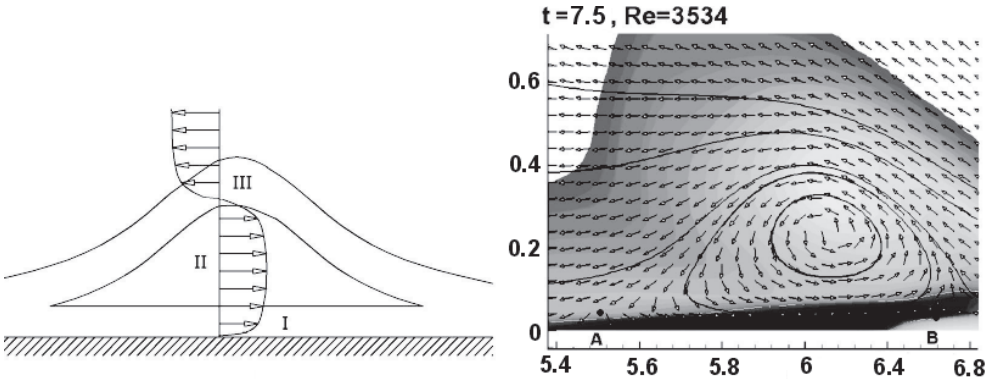


**Figure 8.** (a) The recirculation zone preceding the eruption of the boundary layer according to Van Dommelen and Cowley (1990). (b) The streamlines, the directions of the flow and the vorticity field (greyscale) obtained in the present numerical studies. The vortex patch that induced the recirculation zone is not visible but is located above and has opposite circulation.

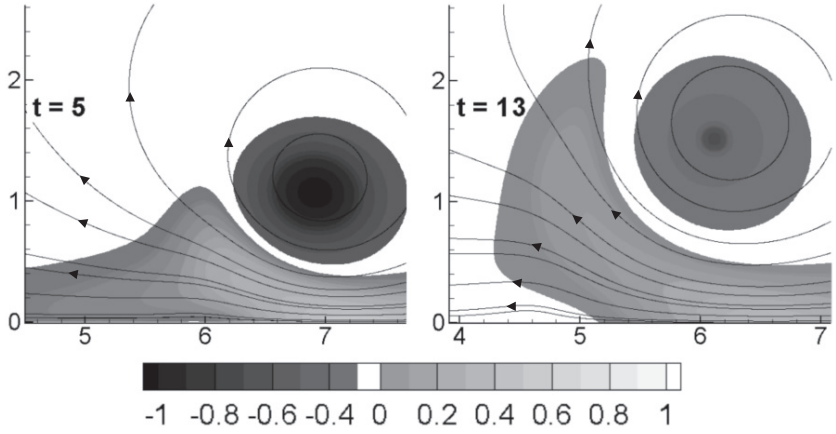


**Figure 9.** Interaction of the vortex patch and the wall, $Re = 500$. There is a lack of recirculation zone. The figure shows the vorticity field with selected streamlines.

MRS condition (see figure 2), unsteady separation takes place when the separation point appears inside the flow. The generation of the recirculation zones does not imply the eruption event. We find that the process of eruption depends on fluid viscosity and on the intensity of the vortex patch. Comparing figure 8(a) with figure 8(b) we note that the recirculation zone in figure 8(b), which qualitatively corresponds to zone 2 on the left, is rotational—the fluid inside it circulates.

The influence of viscosity on the process of eruption is governed by the Reynolds number. With the Reynolds number increasing (and viscosity decreasing) the flow becomes increasingly more complicated.

In figure 9, the vorticity field along with the selected streamlines induced by the vortex patch for Reynolds number $Re = 500$ is presented. In this case, the recirculation zone near the wall has not formed, and consequently there is no separation point. It should be noted that, due to the viscosity of the fluid, vortex particles do not follow the trajectory of the fluid particles.

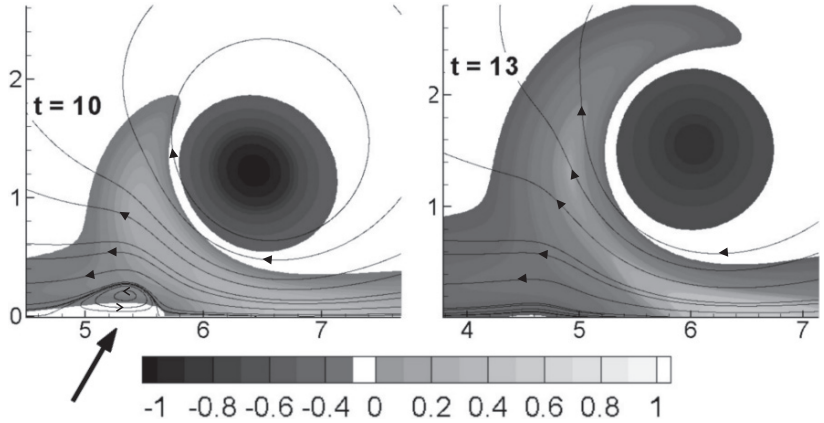


**Figure 10.** Interaction of the vortex patch and the wall, $Re = 1000$. A recirculation zone is visible for $t = 10$ (see the arrow). Further on the recirculation zone disappears. The figure presents the vorticity field with selected streamlines.

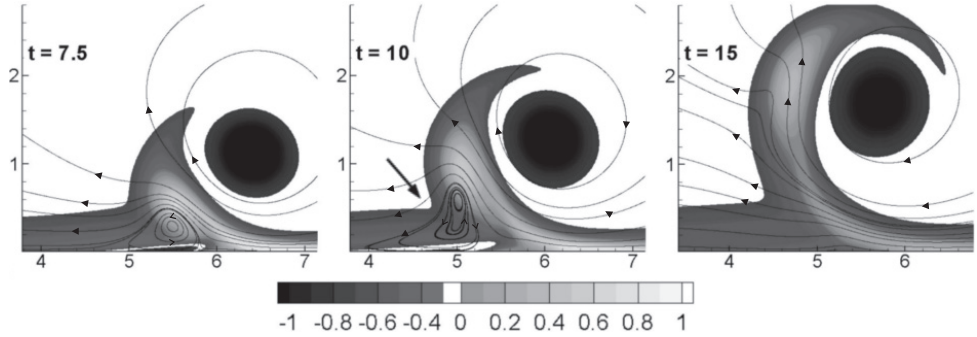


**Figure 11.** Interaction of the vortex patch and the wall, $Re = 4000$. There is a stretching of the recirculation zone for $t = 10$ (see the arrow), but eruption does not take place. The figure shows the vorticity field with selected streamlines.

Increasing the Reynolds number to the value $Re = 1000$, figure 10, results in the appearance of the recirculation zone in the boundary layer but the zone does not develop further because of the high value of the viscosity.

Figure 11 shows the results for $Re = 4000$. Comparing figure 11 with figure 10, we can observe that the emerging recirculation zone is getting intensely stretched in the direction normal to the wall (image $t = 10$). However, the eruption of the boundary layer does not take place yet. The vorticity departing from the wall causes only streamline distortion. The situation changes with the increase of the Reynolds number. For $Re = 5000$ (figure 12), a new phenomenon manifests itself in the flow. It is called the eruption of fluid particles from the boundary layer.

In this case, similarly to the one before, the recirculation zone is intensely stretched in the direction normal to the wall. Splitting of the recirculation zone takes place. Streamlines form a 'figure of 8' shape. Inside the boundary layer, a saddle point is generated (figure 12, $t = 11.25$, and figure 13) that is also a separation point. The process results in the eruption phenomenon, which manifests itself as the ejection of a portion of the fluid from the boundary layer to the

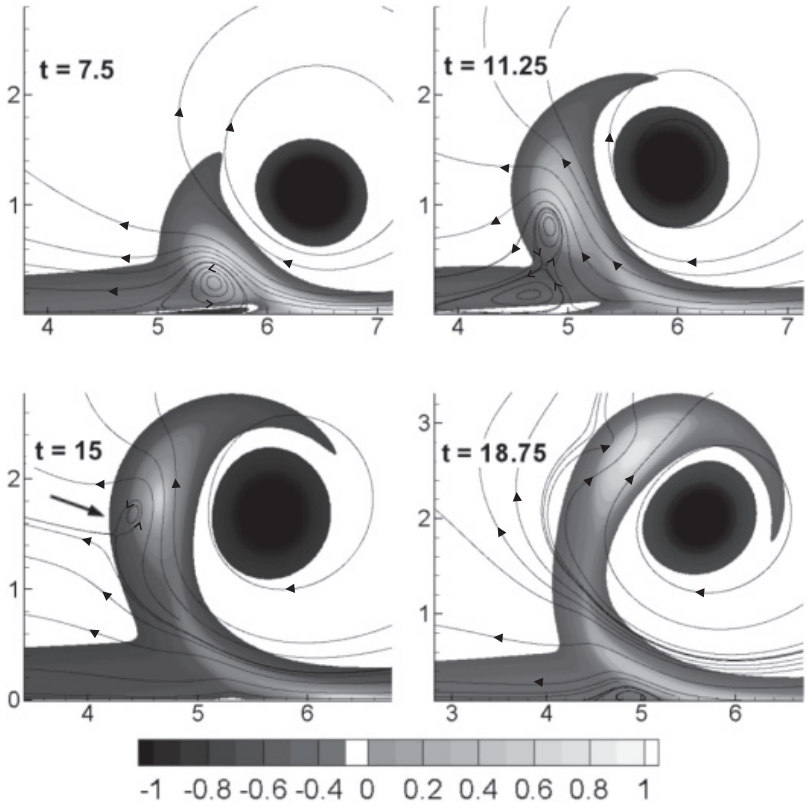


**Figure 12.** Interaction of the vortex patch and the wall, $Re = 5000$. The eruption phenomenon is visible for $t = 15$. The eruption manifests itself as an ejection of fluid elements from the boundary layer to the outer flow. These fluid elements are enclosed in the new vortex structure (closed streamlines, see the arrow).

outer flow. This portion is enclosed in the new vortex structure (closed streamlines) (figure 12, $t = 15$). This means that the separation of the vortex takes place.

Magnified images of the separation phenomenon are shown in figure 13. Attachment points are marked with letter **A**, separation points with **B** and the saddle point with **S**.

In course of time, the recirculation moves along the wall (from right to left) and is stretched slightly (see the $t = 10$ frame). Simultaneously, it is pulled firmly in the normal direction away from the wall. This results in the split of the recirculation zone into two vortex structures. The streamlines close up into a characteristic figure-of-eight shape with saddle point **S** (see the $t = 12.8$ frame). The appearance of the saddle point results in the split of the primary boundary recirculation zone into two independent vortex structures. One of them is lifted upwards and the other remains near the wall, forming a secondary recirculation zone. In course of time, the remaining recirculation zone is dispersed under the influence of viscosity (the $t = 15$ frame). The detachment process of the new vortex is rapid. Fluid particles from the vicinity of the wall are trapped inside the departed vortex.

Figure 14 presents the phenomenon of eruption of the boundary layer for $Re = 10\,000$. In this case, the generated vortex structure on the wall has a high intensity and does not disperse but is going around the primary vortex patch. In figure 14, one can observe the creation of another recirculation zone and eruption (the $t = 28$ and $t = 56$ frames).

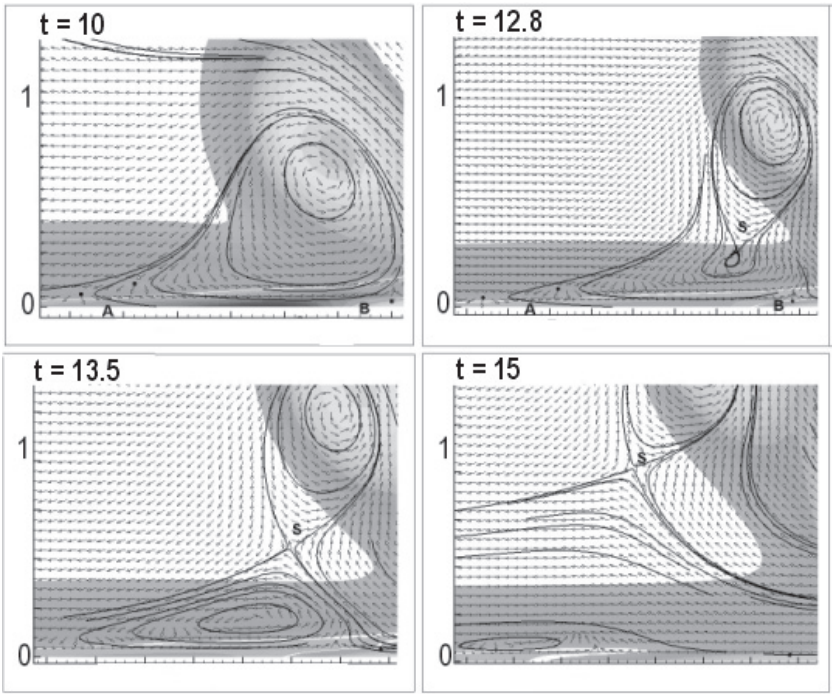


**Figure 13.** The beginning of the eruption process. One can notice the process of the saddle point **S** creation and tearing apart of the recirculation zone. The Reynolds number is as in figure 14 ($Re = 10\,000$).

Raising the Reynolds number results in increasingly more complex flow. Figure 15 presents the results for $Re = 50\,000$. Not only one vortex structure but also a whole sequence of vortex structures detach from the wall (figure 15, frame $t = 84$). For such high values of the Reynolds number, separation of the boundary layer induces highly complex flow near the wall and sheds light on how eruption can influence near-wall turbulence by generating a sequence of vortex structures.

In order to better illustrate the eruption of fluid particles from the wall layer into the main flow, the following numerical experiment was carried out. Along the wall, some passive particles (markers) were placed. Their movement illustrated the evolution of the fluid particles from the wall layer. Markers were placed in four rows. The distance between the rows in the direction normal from the wall was $0.5\Delta y$. So the last row of markers was placed at the height $2\Delta y = 0.02$ from the wall.

Figure 16 presents the evolution of the fluid particles (markers) from the wall layer for $Re = 500$ (compare figure 8). The picture shows that eruption does not take place and that fluid particles remain near the wall. Only the markers from the highest row are moved away slightly by the velocity field induced by the vorticity of the primary vortex patch, but they do not travel far from the wall.

Figure 17 presents the motion of the fluid particles from the wall layer for $Re = 10\,000$ (compare figure 14). In this figure, the eruption phenomenon can be clearly seen. The fluid particles from the boundary layer, enclosed in the vortex structure, are rapidly ejected into the flow (the $t = 11$ and $t = 23$ frames). The first detached vortex is followed by another one (the $t = 37$ frame). The experiment clearly shows that the eruption phenomenon is responsible for transport of fluid particles and vorticity from the wall into the flow.

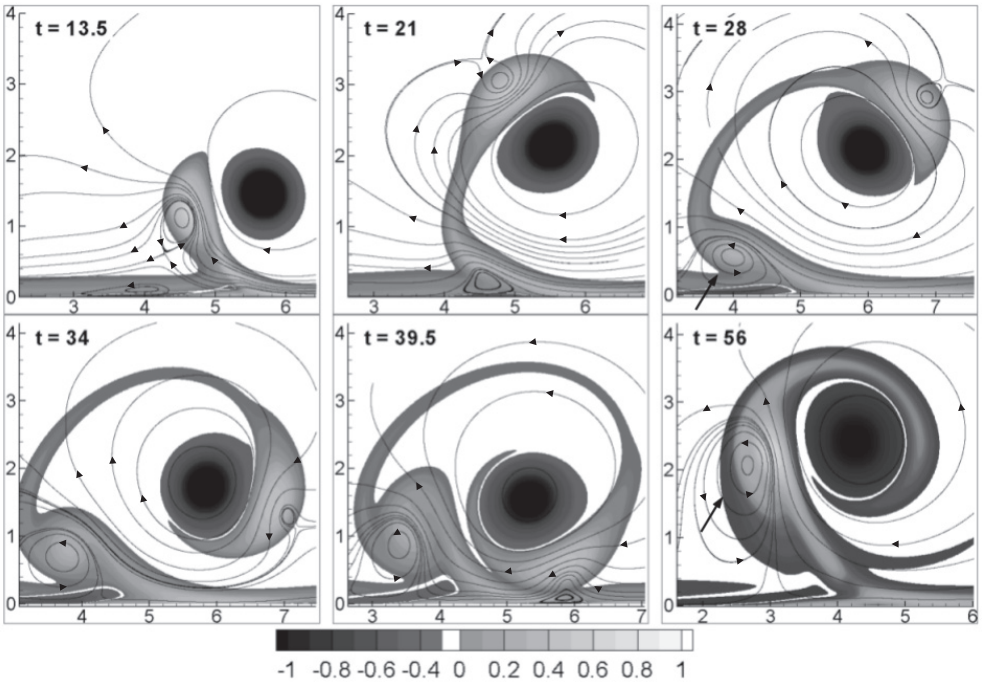


**Figure 14.** The eruption phenomenon, $Re = 10\,000$. One can observe the creation of another recirculation zone ($t = 28$, $t = 56$) (see the arrows).

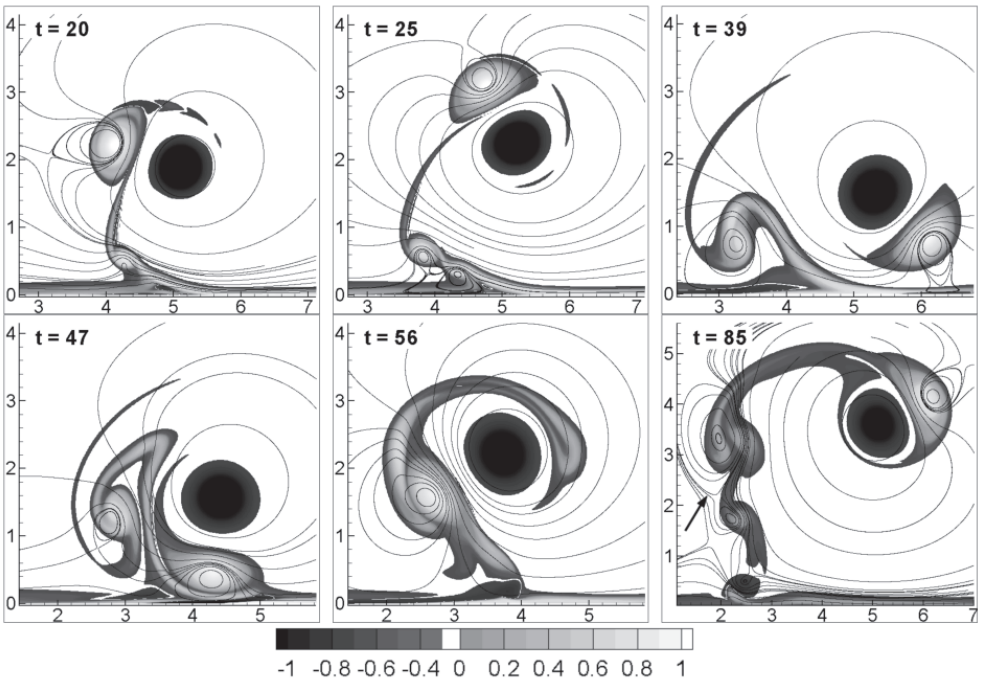


**Figure 15.** The eruption phenomenon, $Re = 50\,000$. Multiple processes of eruption. On can see the sequence of generated vortices $t = 85$ (see the arrow).

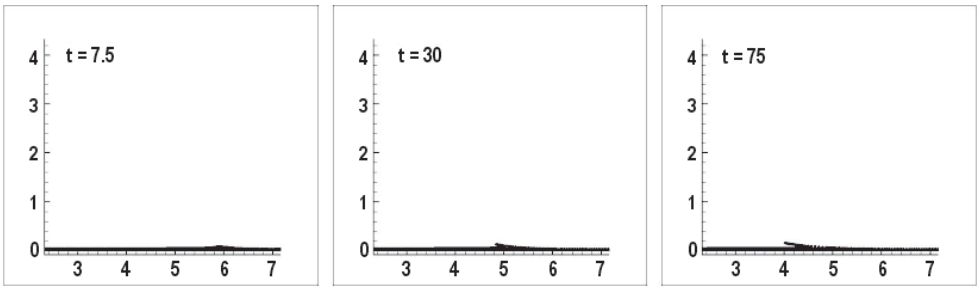


**Figure 16.** Evolution of the fluid particles from the wall layer, $Re = 500$. Eruption does not occur. The figure shows the motion of passive particles (markers).

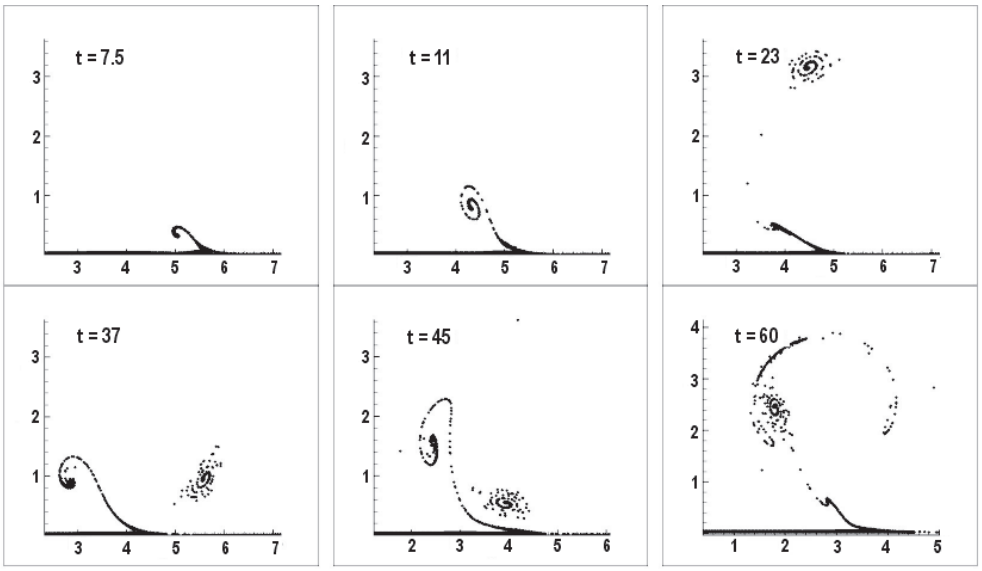


**Figure 17.** Evolution of the fluid particles from the wall layer, $Re = 10\,000$. The eruption phenomenon is clearly visible. The figure shows the movement of passive particles (markers).

## 7. Conclusions

Our numerical results show that the appearance of the recirculation zone (vortex bubble) in the wall layer precedes eruption events. However, such appearance does not always lead to eruption. The eruption process takes place for a sufficiently high Reynolds number (low viscosity). Ejection of the fluid particles from the region close to the wall is preceded by the appearance of a saddle point inside the wall layer. For a sufficiently high Reynolds number the interaction of the vortex patch with the wall may lead to a very complex flow. There appears a cascade of vortices that detach from the wall and move around the primary vortex patch, evoking the sequence of secondary eruption events. One can thus speak about the regenerative nature of the eruption phenomena. It enhances mixing and promotes convective motions. Therefore, better conditions for heat exchange can be achieved by intensifying eruption in the boundary layer. On the other hand, eruptions cause perturbations of the pressure field and may result in noise and other disturbances. The increase of the momentum exchange leads

to the increase of the drag force. In order to reduce the disturbances of the drag force, it is necessary to control and prevent sudden eruptions of the boundary layer.

We have tested thoroughly the method that we used in this work by applying it to a variety of simple test problems: the Poiseuille flow, the second Stokes problem, cavity, backward step flow and vortex dipole interaction with the wall. The obtained results have been published in Kudela and Malecha (2008). It was shown that the rate of convergence of the method was $\sim$1.5. The obtained results were in good agreement with experimental data and other numerical methods. The vortex-in-cell method can be extended to 3D problems (Cottet and Poncet 2003, Ould-Salhi *et al* 2000). Our next step is to investigate the eruption phenomenon for 3D flows.

## Acknowledgments

We acknowledge financial support from the Polish Ministry of Education and Sciences under grant number 3 T10B 048 30. We thank Professor Konrad Bajer from Warsaw University for a review of this paper and help with language corrections.

## References

Batchelor G 1970 *An Introduction to Fluid Dynamics* (Cambridge: Cambridge University Press)
Bradshaw P 1996 *Prog. Aerosp. Sci.* **32** 575–624
Chorin A 1973 *J. Fluid Mech.* **57** 785–96
Cottet G and Koumoutsakos P 2000 *Vortex Method: Theory and Practice* (Cambridge: Cambridge University Press)
Cottet G and Poncet P 2003 *J. Comput. Phys.* **193** 136–58
Cowley S, Van Dommelen L and Lam S 1990 *Phil. Trans. R. Soc.* A **333** 343–78
Doligalski T, Smith C and Walker J 1994 *Annu. Rev. Fluid Mech.* **26** 573–616
Doligalski T and Walker J 1984 *J. Fluid Mech.* **139** 1–28
Jimenez J and Moin P 1991 *J. Fluid Mech.* **225** 213–26
Koumoutsakos P 1993 Direct numerical simulations of unsteady separated flows using vortex methods *PhD Thesis* California Institute of Technology
Koumoutsakos P, Leonard A and Pepin F 1994 *J. Comput. Phys.* **113** 52–61
Kudela H and Malecha Z 2007 *J. Theor. Appl. Mech.* **45** 785–800
Kudela H and Malecha Z 2008 *Task Q.* **13** 15–32
Landau L and Lifszyc E 1994 *Hydrodynamika* (Warszawa: Wydawnictwo Naukowe PWN)
Lighthill M 1963 *Introduction. Boundary Layer Theory* ed J Rosenhead (Oxford: Oxford University Press)
Ould-Salhi M, Cottet G and El Hamraout M 2000 *J. Sci. Comput.* **22** 1655–74
Panton R 2001 *Prog. Aerosp. Sci.* **37** 341–83
Peridier V, Smith F and Walker J D A 1991a *J. Fluid Mech.* **232** 99–131
Peridier V, Smith F and Walker J D A 1991b *J. Fluid Mech.* **232** 133–65
Perry A and Chong M 1982 *J. Fluid Mech.* **119** 173–217
Prandtl L 1905 *Verhandlg. III. Intern. Math. Kongr. Heidelberg* pp 574–84
Robinson S 1991 *Annu. Rev. Fluid Mech.* **23** 601–39
Rott N 1956 *Q. Appl. Math.* **13** 444–51
Schlichting H 1979 *Boundary-Layer Theory* (New York: McGraw-Hill)
Sears W 1956 *J. Aeronaut. Sci.* **23** 490–99
Smith C R and Walker D A 1996 Turbulent wall-layer vorticies *Fluid Vortices* (Dordrecht: Kluwer) chapter IV
Telionis D 1981 *Unsteady Viscous Flow* (New York: Springer)
Van Dommelen L and Cowley J 1990 *J. Fluid Mech.* **210** 593–626
Walker J 1978 *Proc. R. Soc.* A **359** 167–88
Wu J Z, Ma H Y and Zhou M D 2006 *Vorticity and Vortex Dynamics* (Berlin: Springer)